Porous Exfoliated Poly(ε-caprolactone)/Clay Nanocomposites: Preparation, Structure, and Properties

Oana M. Istrate,[1,2] Biqiong Chen[1,2]

[1]*Department of Mechanical and Manufacturing Engineering, Trinity College Dublin, College Green, Dublin 2, Ireland*
[2]*Trinity Centre for Bioengineering, Trinity College Dublin, Dublin 2, Ireland*

Received 22 August 2011; accepted 29 September 2011
DOI 10.1002/app.36336
Published online 27 December 2011 in Wiley Online Library (wileyonlinelibrary.com).

ABSTRACT: Porous biodegradable poly(ε-caprolactone) (PCL)/clay nanocomposites were prepared by incorporating a blowing agent into the galleries of an organoclay, followed by mixing the pretreated organoclay and PCL to give partially intercalated and exfoliated nanocomposites and subsequently degrading the blowing agent *in situ* to increase the exfoliation degree in the porous nanocomposites. The blowing agent played dual roles in the foaming process: formation of bubbles and facilitation of clay exfoliation, which were confirmed by X-ray diffraction and transmission electron microscopy. Such porous nanocomposites possessed significantly more uniform porous structures and smaller pore sizes compared to their polymer counterparts, which were characterized by X-ray micro computed tomography. They also exhibited increases of the thermal degradation temperature by 41°C, the compressive modulus by 152%, and the compressive stress at 10% strain by 177%. The relative modulus-relative density relationship of the porous nanocomposites was found to follow the Mills–Zhu model for closed cells. Such porous biocompatible and biodegradable nanocomposites will find potential applications in, for example, carriers of chemicals, drugs, and medical and diagnostic devices.
 J Appl Polym Sci 125: E102–E112, 2012

Key words: biopolymer; blowing agents; clay; foams; nanocomposites

INTRODUCTION

Past years have marked a turning point in polymer foaming, some of the commodity plastics, known for their biochemical endurance, being replaced by biodegradable polymers, for example, poly(ε-caprolactone) (PCL), poly(lactic acid) (PLA), and poly(glycolic acid). Possessing the ability to degrade upon bioactive environment exposure into small molecules, for example, water, CO_2, and biomass,[1] these polymers may represent a possible solution to the growing waste problem that the world is facing.[2] Lately, biodegradable polymers have been used for a series of packaging and biomedical applications, for example, drug-delivery systems, bioabsorbable surgical sutures, tissue engineering scaffolds, and temporary internal fixation of a variety of tissue damages.[3,4]

A number of conventional polymers, such as low-density polyethylene,[5,6] polypropylene,[7] polystyrene,[8] poly(vinyl chloride),[9] and poly(ethylene terephthalate),[10] and biodegradable polymers such as PCL[11,12] and PLA,[13] have been foamed using different chemical[14–16] or physical[5,6,8,11] blowing agents for various applications.[7,11] Compared to traditional cellular polymers, porous biodegradable polymers often present low stiffness, brittleness, and/or high-gas permeability.[17] Recent research shows that strength, stiffness, thermal stability, and barrier properties of biopolymers can be greatly improved with the addition of a small amount of nanoclay.[18–20] For example, Chen and Evans[20] observed that a content of 4.2 wt % organoclay (Bentone®105) platelets increased the tensile strength, Young's modulus, and elongation at break of PCL by 88, 23, and 216%, respectively, the addition of clay leading to the occurrence of polymeric materials characterized by superior mechanical properties. By using 5 wt % organoclay (Cloisite® 30B), Ludueña et al.[18] found that the stiffness of a cast PCL film, with intercalated and exfoliated structures, was enhanced by 47% compared to the pristine polymer film, while the crystallinity increased from 58 to 63%. Using the same concept, the properties of biopolymer porous materials may also be improved. For instance, Liu et al.[12] showed that 5 wt % organoclay (Nanolin® DK2) dispersed in PCL renders partially intercalated and partially exfoliated nanostructures in which the subsequent incorporation of a chemical blowing

Additional Supporting Information may be found in the online version of this article.

Correspondence to: B. Chen (chenb@tcd.ie).

Contract grant sponsor: Environmental Protection Agency; contract grant number: EPA-2008-PhD-WRM-4.
Contract grant sponsor: European Union; contract grant number: 026019 ESTEEM.

agent led to porous materials that presented 60% increase in compressive modulus compared to the pristine porous polymer.

Because clay is ubiquitous in nature, environmentally friendly, and biocompatible,[21] using it as nanofiller for biodegradable and biocompatible porous polymers results in the formation of green and biomedical nanocomposites with enhanced properties.[4] This relatively new class of materials represents a viable alternative to conventional porous polymers used for packaging and biomedical applications.

There are three common approaches for preparing polymer/clay nanocomposites: *in situ* polymerization, solvent method, and melt processing, which are known to lead to intercalated and/or exfoliated structures.[22] The former is characterized by the presence of polymer between stacked clay layers, which causes the occurrence of tactoid structures, while the latter presents total delamination of the clay platelets.

The previous research on porous polymer/clay nanocomposites, including biopolymer-based foams, was mainly concerned with the materials manufactured by mixing the polymer, clay, and blowing agent [physical, e.g., CO_2, N_2, or a combination of both[11] or chemical, e.g., azodicarboxamide (ADC), sodium bicarbonate (SB), or zinc carbonate][14] simultaneously,[15] with the blowing agent playing the sole role of creating bubbles. This work aimed to give the blowing agent a second role by preincorporating a chemical blowing agent into the clay galleries and expanding the clay galleries during bubble formation, hence offering the clay a higher degree of exfoliation and the resultant porous materials better properties as opposed to existing porous nanocomposites with comparable material compositions. Semicrystalline PCL was selected as the matrix because of its ductility, biocompatibility, and wide range of biomedical applications such as drug-delivery systems, wound dressings and sutures, and bioresorbable implants.[3,17,23,24] SB and ADC, known for their low toxicity and progressive gas yield,[16] were chosen as blowing agents. The structures were investigated by X-ray diffraction (XRD), transmission electron microscopy (TEM), and X-ray micro computed tomography (Micro-CT), thermal properties and crystallinities were studied by thermal gravimetric analysis (TGA) and differential scanning calorimeter (DSC), and mechanical properties were obtained from compression testing.

EXPERIMENTAL

Materials

Poly(ε-caprolactone), $\overline{M}_n$ = 70,000–90,000, was purchased from Sigma-Aldrich. A commercially available organoclay, Cloisite 30B (C30B), that is, a methyl, tallow, bis-2-hydroxyethyl, quaternary ammonium modified montmorillonite, was generously supplied by Southern Clay Products (Texas, USA). The cation exchange capacity was 90 meq/100 g clay, the density was 1980 kg m^{-3}, and the inorganic content was 70%. Reagent-grade SB, $NaHCO_3$ and ADC, and $C_2H_4O_2N_4$ were purchased from Sigma-Aldrich. Because of the high-decomposition temperature[14] of ADC, zinc oxide (ZnO; Analytical grade) from Sigma-Aldrich was used to activate the blowing agent and reduce the decomposition time.[25] Tetrahydrofuran (THF) was used as a solvent. All materials were used as received.

Clay treatment

C30B was pretreated with two chemical blowing agents, namely SB and ADC/zinc oxide to give the SB- and ADC-treated clays. In both cases, 6.5 g of C30B was first dispersed overnight, under constant stirring, in 325 mL of THF : H_2O = 1 : 1 (v/v) to produce a clay suspension. For the SB-treated clay, a 2.5 wt % (w/w) solution of SB in distilled water was added to the clay suspension. For the ADC-treated clay, the clay suspension was mixed with a 5 wt % (w/w) solution of ADC : ZnO = 1 : 1 (w/w) in distilled water. To achieve a good dispersion of ADC and ZnO in water, the solution was ultrasonicated for 1 h before being added to the organoclay suspension. The treated-clay suspensions were kept under constant stirring for ~ 24 h and dried in an oven for 8 h at 80°C, followed by being grounded into fine powders.

Preparation of porous PCL/clay nanocomposites

Porous PCL-treated clay nanocomposites were obtained in two steps, preparation of solid nanocomposites and thermal degradation of the blowing agent to create pores. In the first step, polymer/clay nanocomposites with 5.8 wt % blowing agent-treated organoclay were prepared following the procedure described below. First, the blowing agent-treated organoclay was dispersed in THF to obtain a 3 wt % clay dispersion. Separately, PCL was dissolved in the same solvent to create a 10 wt % solution. Then, the clay dispersion was mixed with the PCL solution at predetermined volumes at room temperature for 2 h on a magnetic stirring plate and ultrasonicated for 1 h. Finally, the resulting mixture was cast and dried at room temperature in a fume cupboard to obtain the solid nanocomposite.

In the second step, the nanocomposites were compression molded in a cylindrical mold on a hot plate at 150°C for 1 h. The mold was then covered and inserted in an oven for 1 h at 190°C for SB-treated

clay and at 210°C for ADC-treated clay, temperatures that were predetermined, from the TGA results, as the optimal foaming conditions for both blowing agents. Porous PCL samples without clays were prepared following a protocol similar to the one described earlier. However, in these cases, 30 min at a temperature of 115°C on the hot plate were sufficient, while the oven temperatures were lowered to 170 and 190°C for SB and ADC, respectively.

Characterization

XRD was carried out on a Phillips PW1720 X-ray diffractometer with a Cu $K_{\alpha 1}$ ($\lambda = 0.15406$ nm) anode tube at the standard conditions of 40 kV and 20 mA. Clay powders and thin discs of nanocomposites before and after foaming were tested from 2° to 10°, 2θ angle, at a step size of 0.02° and duration of 2.5 s per step.

TEM was performed on a TECNAI G2 20 twin electron microscope for porous polymer/clay nanocomposites and on a JEOL JEM-2010 for nonporous polymer/clay nanocomposites. The specimens were sectioned using a Reichert-Jug "Ultracut" or a NOVA ultramicrotome equipped with a diamond knife. The sections (~ 100 nm in thickness) were collected in a trough filled with water and placed on a 200 mesh copper grid for porous solids and 400 mesh titanium grids for nonporous samples.

FTIR spectra were realized on a FT-NIR instrument (Perkin Elmer Spectrum One NTS) equipped with ATR Sampling Accessory. The samples were run from 650 to 4000 cm^{-1} at a resolution of 2 cm^{-1}.

TGA was performed on a Perkin Elmer Pyrus 1 TGA equipped with an ultramicro balance with a sensitivity of 0.1 μg, under air flow, from 100 to 650°C at a heating rate of 10°C min^{-1}.

DSC was carried out on a Perkin Elmer Diamond DSC at a scan rate of 20°C min^{-1}. The crystallinity of the porous and nonporous polymer/clay nanocomposites was calculated, using eq. (1)[12] and considering the melting enthalpy of the sample (ΔH_m) from the second heat scan in order to eliminate the effects of the heating history.

$$\chi_c(\%) = \frac{\Delta H_m}{\mu_p \times \Delta H_m^0} * 100 \quad (1)$$

where μ_p is the weight fraction of PCL in the nanocomposite sample and $\Delta H_m{}^0$ is the melting enthalpy for the 100% crystalline PCL, that is, 136 J g^{-1}.[26]

Micro-CT was run on a Scanco Micro-CT 40 Scanner (Scanco Medical AG) at the standard resolution (acquisition: 250 projections per 180° with 1024 samples each, an energy of 55 kVp and a current of 145 μA). The micrographs were realized using a predefined threshold that was found to give the most accurate interpretation of the image throughout the whole scan in order to assess the structure and porosity. The Image J software was used to analyze the pore size. For each micrograph, a substantial number of pores were measured, and the mean and standard deviation normalized for 20 pores with a 95% confidence level are presented.

Compressive tests were carried out on an Instron 8501 universal testing machine with a load of 100 kN at a rate of 1 mm min^{-1}. Testing was arbitrarily terminated at the deformation of 60% according to ASTM C365-05. Five surface-ground cylindrical specimens with a diameter of 19 mm and a height of ~ 10 mm were tested for each type of the porous solids. The mean and standard deviation values reported present a confidence level of 95%. Statistical significance was assessed by a two-tailed, Type II "t" test with a criterion that the probability of a difference in means due to chance is less than 0.05. The bulk density of the porous solids was calculated as the ratio of the weight to the volume of each sample. The diameter and height of each cylindrical specimen were measured with a Vernier caliper in at least three points, while the weight was measured on an analytical balance. Five specimens were weighed and measured for each of the porous solids considered. The mean and standard deviation values reported present a confidence level of 95%.

RESULTS AND DISCUSSION

Structure

Figure 1 shows the XRD patterns of the organoclay, the blowing agent-treated organoclays, and the PCL/treated organoclay nanocomposites, before and after foaming. The untreated organoclay (Curve 1) presented a peak at $2\theta = 4.8°$, corresponding to a basal plane spacing, d_{001}, of 1.85 nm. By modifying the clay with the blowing agents, d_{001} remained the same for ADC [Fig. 1(A), Curve 2], while, for SB, it slightly decreased [Fig. 1(B), Curve 5] probably due to removal of some surfactant molecules or impurities from the galleries. As the molecular sizes of the blowing agents are smaller than the one of the surfactant, their entrance, if available, may not increase the gallery spacing. To further characterize the structures of the treated organoclays, FTIR was used, and the results are shown in Figure 2. When the organic blowing agent was used to modify the organoclay, the position of the Si—O stretching band[27] in the organoclay (Curve 1) shifted from 1004 to 1010 cm^{-1} in the ADC-treated clay (Curve 5) due to hydrogen bonding with the carbonyl groups present in ADC.[28]

Although the XRD spectrum does not present a shift toward a lower 2θ angle, the FTIR results might

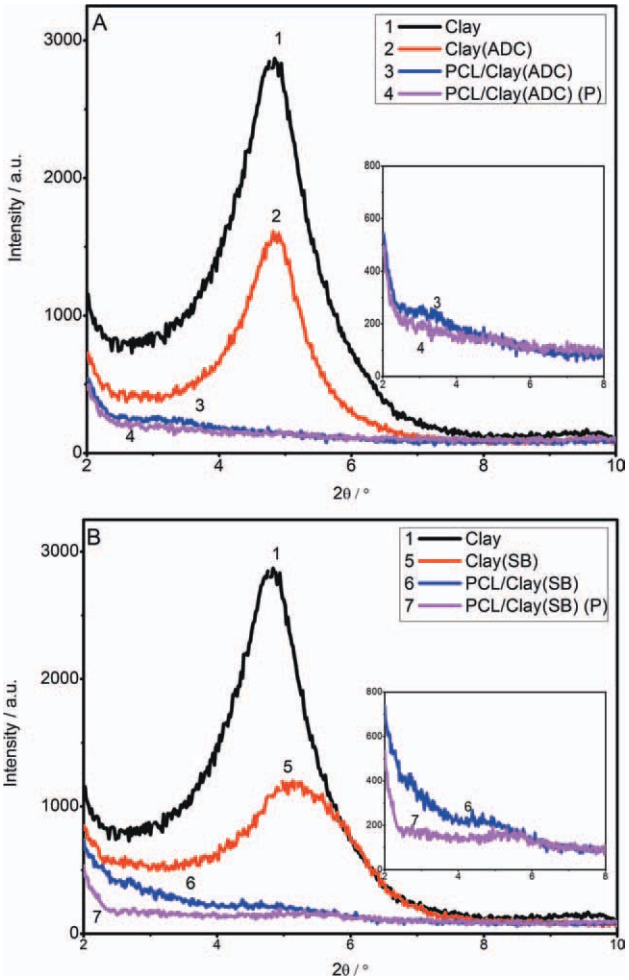

Figure 1 XRD traces for clays and nanocomposites. 1. Clay (C30B), 2. Clay(ADC), 3. PCL/Clay(ADC), 4. PCL/Clay(ADC) (P), 5. Clay(SB), 6. PCL/Clay(SB), and 7. PCL/Clay(SB) (P). [Color figure can be viewed in the online issue, which is available at wileyonlinelibrary.com.]

indicate a change inside the clay gallery, suggesting that the ADC molecules could have entered the gallery, resulting in strong interactions with the clay. This postulation was supported by the shifts that occurred in the water bands present inside the clay gallery (Curve 1). The band at 3429 cm^{-1}, characteristic to stretching of the interlayer water,[29,30] shifted to 3150 cm^{-1} (Curve 5). The shift was due to hydrogen bonding between the water molecules and stretching of the N—H bonds in the ADC molecules. Similar changes were observed when SB was used to treat the organoclay, with the two peaks designated to the interlayer water at 1639 and 3429 cm^{-1},[29,30] shifting to 1684 and 3459 cm^{-1} (Curve 3). The changes in the absorption peaks observed via FTIR indicated that the clay treatment has been successful and that, in both cases, the blowing agents have entered the clay's gallery.

For the blowing agent-treated organoclays dispersed into PCL, the d_{001} peaks presented in the treated organoclays were found to shift toward smaller 2θ values and/or diminish their intensity considerably (Fig. 1, Curve 1 vs. Curves 3 or 6), suggesting the co-existence of intercalated and exfoliated structures, which was subsequently confirmed from the TEM results. Upon foaming, the intensity of the peaks was further diminished (Fig. 1, insets), initially indicating an increase in the exfoliation degree.[22] Figure 3 shows the TEM images of PCL/treated clay nanocomposites before and after foaming. As it can be observed from Figure 3(A), the clay layers appeared mainly as intercalated tactoids with occasional exfoliated single clay platelets before foaming. The intercalated structures were found to have between two and seven layers with an average of four clay platelets per stack (determinate from over 10 stacks, with a 95% confidence interval). The few exfoliated clay platelets were either ordered [Fig. 3(A), inset] or disordered. Partially intercalated and partially exfoliated clay platelets in PCL/clay nanocomposites have been previously reported by Liu et al.[12] for 5 wt % DK2 (a montmorillonite modified by methyl tallow bis-2-hydroxyethyl ammonium, the surfactant being the same as for C30B) and Ludueña et al.[18] for 2.5, 5, and 7.5 wt % C30B.

Analyzing the structures that occurred in porous PCL/blowing agent-treated clay nanocomposites [Fig. 3(B,C)], it is confirmed that the enhancement in the exfoliation degree is dependent on the blowing agent used to treat the clay. The insertion of inorganic blowing agent molecules inside the clay gallery resulted in well-dispersed clay platelets with ordered and disordered full exfoliation [Fig. 3(B), inset]. Ordered exfoliated and single delaminated clay layers were also observed when organic blowing agent molecules were used to treat the clay. However, in this case, 40% of nanostructures were found to be intercalated structures with an average of two layers per stack and a basal spacing of 2.9 nm [Fig. 3(C), inset], with the remaining 60% being fully exfoliated. Nevertheless, these results revealed that, in both the cases, the exfoliation and dispersion of clay platelets were improved remarkably after the blowing agent was degraded in clay galleries.

The type of blowing agent used influenced the amount of gas dispersed and the viscosity of the melt.[11,14] The inorganic blowing agent produced, upon degradation (Scheme 1), nonpolar carbon dioxide (CO_2), and water molecules that were released inside the clay gallery. Combining the high solubility of CO_2 in water and the polar nature of the water molecules,[31] the degradation product presented a high affinity for the hydrophilic clay platelets and a high diffusivity in the polymer,[32] which led to the occurrence of fully exfoliated porous polymer/clay nanocomposites. The nonpolar nitrogen molecules (N_2) that the organic blowing agent yielded upon

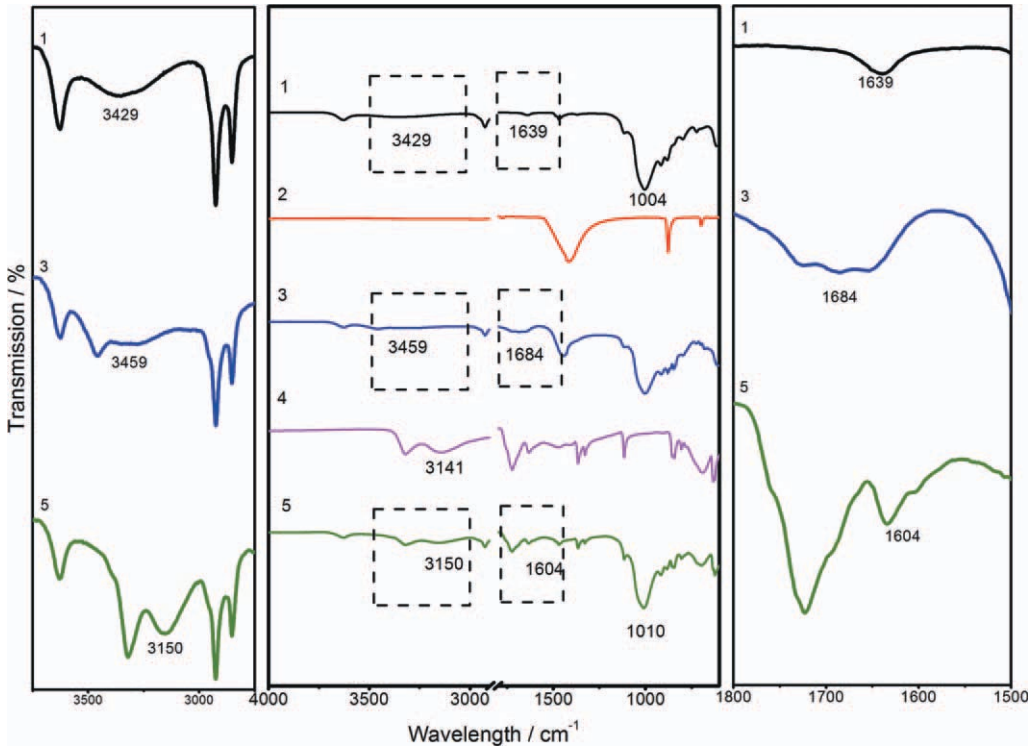

Figure 2 FTIR spectra for treated organoclays and related materials: 1. C30B, 2. SB, 3. Clay(SB), 4. ADC and 5. Clay(ADC). [Color figure can be viewed in the online issue, which is available at wileyonlinelibrary.com.]

decomposition (Scheme 1) resulted in intercalated/exfoliated nanocomposites. The process of obtaining highly exfoliated porous polymer/clay nanocomposites was summarized in Scheme 2. First, the organoclay was treated with an inorganic blowing agent. This allowed the small blowing agent molecules to enter the clay gallery mainly due to hydrogen interactions between the blowing agent and the interlayer water. Second, the treated clay was dispersed in the polymer matrix via the solution method. This step permitted PCL chains to penetrate inside the clay gallery, which resulted in mostly intercalated and minor exfoliated nanocomposite structures [Fig. 3(A)]. Finally, the PCL/blowing agent-treated clay nanocomposites were exposed to higher temperatures, which degraded the blowing agent according to Scheme 1. The production of gas inside the clay gallery expanded the basal spacing further, leading to fully exfoliated porous nanocomposites in the case of using SB as the blowing agent and highly dispersed porous nanocomposites when ADC was used instead of SB.

The effects of the treated organoclays on the microstructure of the porous PCL were investigated.

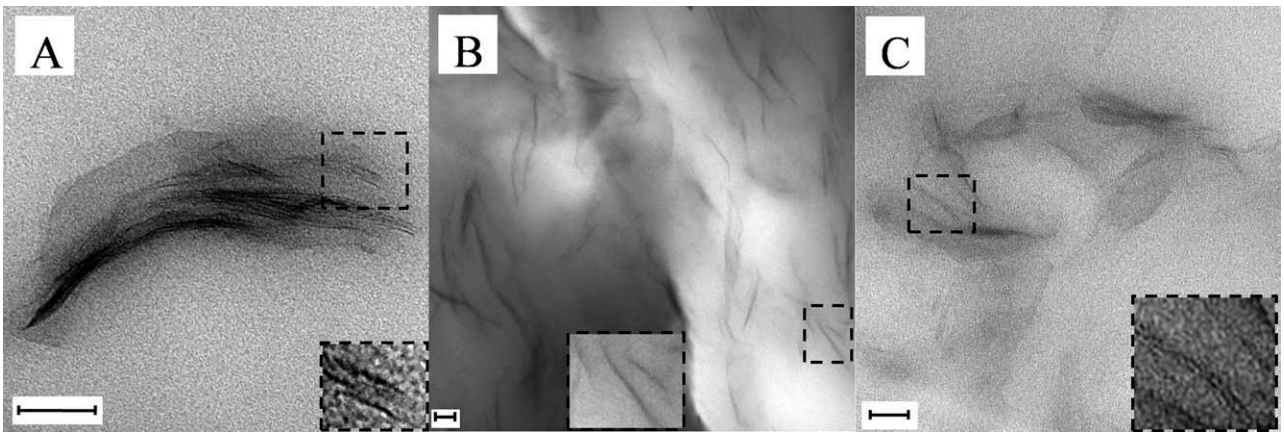

Figure 3 TEM images of: A. PCL/Clay(SB) nanocomposite, B. porous PCL/Clay(SB) nanocomposite and C. porous PCL/Clay(ADC) nanocomposite (Scale bar: 100 nm for the main figures and 25 nm for the insets)

$$2\,NaHCO_3 \longrightarrow Na_2CO_3 + CO_2\,(g) + H_2O\,(g)$$

$$C_2H_4O_2N_4 \longrightarrow N_2\,(g) + CO\,(g) + CO_2\,(g) + NH_3\,(g)$$

Scheme 1 Thermal decomposition of blowing agents.

The structure, presented in micro-CT scans in Figure 4, appeared to be irregular in the absence of clay [Fig. 4(A,B1)], throughout the entire sample [Fig. 4(B2)]. The pore dimensions of the porous solids were characterized by a wide range of values due to the high number of gas molecules produced.[16] By adding the blowing agent-treated organoclays, relatively uniform structures were formed and observed in section [Fig. 4(D1) vs. 4(B1)] and throughout the entire specimen [Fig. 4(D2)]. The clay-filled porous solids presented 39 and 46% reductions in pore size, with statistical significance, for SB and ADC (Table I, Column 3). These changes may be attributed to the ability of clay to act as a nucleating agent[12] and presumably to create a barrier effect,[34] inhibiting cell growth[23] and demonstrating that clay plays an essential role in controlling the cellular structure.[12]

The density of the porous PCL/clay nanocomposites (ρ_f, Table I, Column 4) increased, by up to 40%, compared to their respective polymer counterparts. The density of solid polymer/clay nanocomposites (ρ_s, Table I, Column 5) was calculated according to the equations presented in the Supporting Information section and considering that the clay platelets were fully exfoliated when the inorganic blowing agent was used to treat the organoclay as it was observed from the TEM images [Fig. 3(B)] and intercalated/exfoliated in the case with the organic blowing agent according to the TEM images [Fig. 3(C)]. For these calculations, values of 1980, 3100, and 1140 kg m^{-3} (Ref. 35) were used as the densities of organoclay, clay platelets, and PCL. The amount of surfactant adsorbed on the surface of the clay platelets was not considered in the solid density calculation, because the difference in the densities of the surfactant and of the polymer was too small to have an impact on the solid density.[36] The solid density of the polymer-blowing agent systems was taken as the density of the solid PCL, that is, 1140 kg m^{-3}, due to the insignificant amount of the residual blowing agent present in the systems ($\sim$ 1.5 wt %). The porosities presented in Column 6 were calculated from the densities of the porous materials and their corresponding solid densities, that is, $1 - \rho_f/\rho_s$.

As it can also be observed from Table I, the porosity and pore size of the porous materials varied with the blowing agent used. The porous PCL obtained with ADC showed a pore size and porosity 212 and 178% higher than the porous PCL(SB). This is a consequence of lower gas yield and poorer blowing efficiency that the inorganic blowing agent, SB, has in contrast to the organic blowing agent,[15] and the high solubility that the CO_2 produced by SB has compared to the N_2 produced by ADC (Scheme 1).[11] The relative densities (ρ_f/ρ_s) were found to be 0.74 for PCL/Clay(SB) (P) and 0.45 for PCL/Clay(ADC) (P). Because they are higher than 0.1, the materials cannot be considered as low-density foams, but structural foams ($0.4 < \rho_f/\rho_s < 0.8$)[37] or porous solids ($0.3 < \rho_f/\rho_s$).[38]

Crystallinity and thermal properties

The crystallinity and thermal properties of nonporous and porous polymers and polymer/clay nanocomposites were affected by the addition of clay and the type of blowing agent used. Table II shows that the crystallization temperature (Column 2) of PCL increased by 10.1°C by the addition of SB-treated clay. The degree of crystallinity (Column 3) increased from 43.9% in PCL(SB) to 49.7% in PCL/Clay(SB), which may be attributed to the nucleating effect of clay on crystallization.[12] However, not the

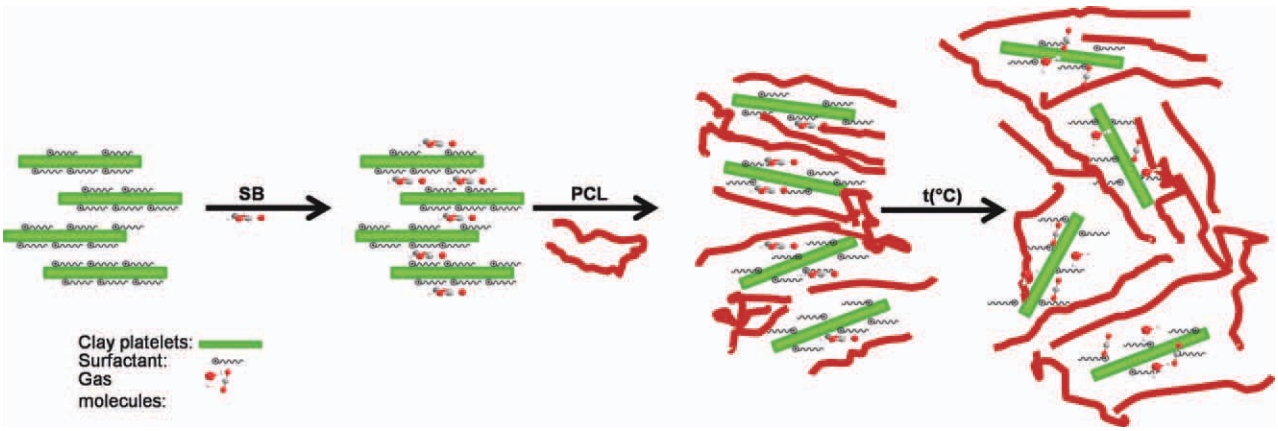

Scheme 2 Exfoliation process in porous PCL/blowing agent-treated organoclay nanocomposites. [Color figure can be viewed in the online issue, which is available at wileyonlinelibrary.com.]

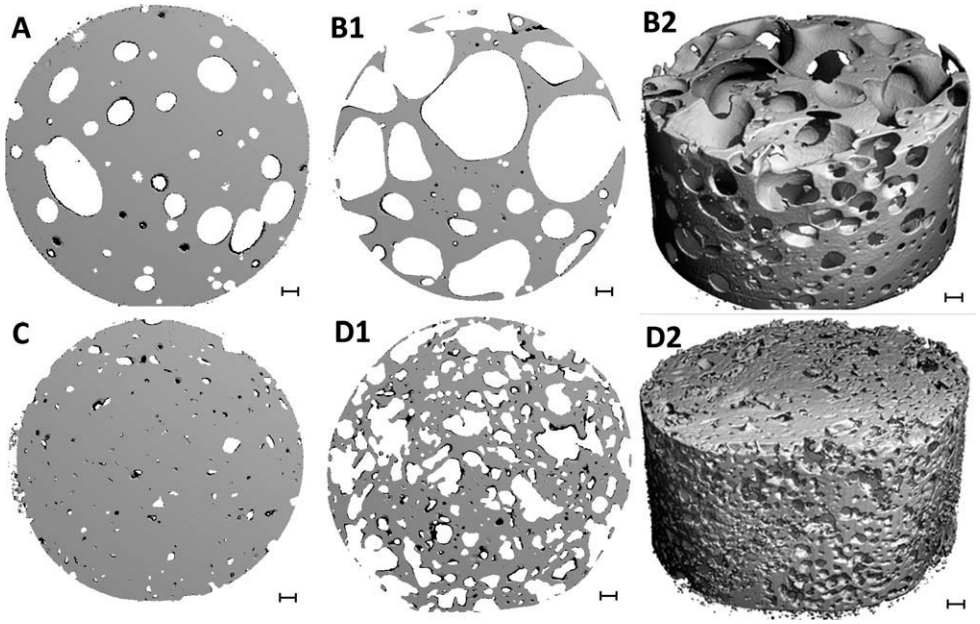

Figure 4 Micro-CT scans for porous solids: A) PCL(SB) (P), B) PCL(ADC) (P), C) PCL/Clay(SB) (P), and D) PCL/Clay(ADC) (P) (Sections A, B1, C and D1: 5 slices; Scale bar: 1 mm).

same effects were observed when ADC was used to treat the clay, the crystallization temperature and crystallinity remaining almost unchanged with the inclusion of clay. After foaming, the porous PCL(SB) presented similar changes in the crystallization temperature and the crystallinity with the presence of clay to the cases in its counterpart before foaming. Again not the same effects were observed for the porous PCL(ADC). The use of organic blowing agent with an activator to treat the organoclay led to a slight decrease in the crystallization temperature and the crystallinity. The variations in the crystallinity by the addition of clay can be accounted for by two factors nucleation that increases crystallinity and reduction in the flexibility of polymer molecular chains that impedes rearrangement of macromolecular chains into ordered crystalline structures and hence reduces crystallinity. Both factors are related to clay dispersion and content. The higher crystallinity in the porous PCL/Clay(SB) and lower crystallinity in the porous PCL/Clay(ADC) compared to their respective porous PCL suggest nucleation effect prevails in the former whereas chain stiffening effect dominates in the latter.

The thermal degradation behaviors for PCL/treated clay nanocomposites before and after foaming were analyzed by TGA. From the derivative thermogravimetric curves in Figure 5, it can be observed that before foaming [Fig. 5(A)], the presence of clay platelets increased the degradation temperature (i.e., the peak temperature observed) from 363°C in PCL(SB) to 397°C in PCL/Clay(SB), and from 390°C in PCL(ADC) to 400°C in PCL/Clay(ADC). The enhancements in the degradation temperature with the clay addition were due to strong bonding between the polymer and the clay. The higher degradation temperature recorded for PCL(ADC) compared to PCL(SB) may be ascribed to the presence of the ZnO molecule that prevents degradation.[39] A similar variation was observed by Liufu et al.[39] for

TABLE I
Pore Sizes, Densities, and Porosities of Porous PCL and PCL/Clay Nanocomposites

Sample ID	Material	Pore size (mm)	Foam density (kg m^{-3})	Solid density (kg m^{-3})	Porosity[a] (%)
PCL(SB) (P)	PCL foamed with SB	0.57 ± 0.20	851 ± 30	1140[b]	23.6
PCL/clay (SB) (P)	PCL/SB treated clay nanocomposites, foamed	0.35 ± 0.07	882 ± 130	1189	25.8
PCL(ADC) (P)	PCL foamed with ADC	1.78 ± 1.12	392 ± 170	1140[b]	65.6
PCL/clay (ADC) (P)	PCL/ADC treated clay nanocomposites, foamed	0.96 ± 0.10	549 ± 11	1229	55.3

[a] Calculated from densities of foams and solids presented in Columns 4 and 5.
[b] From literature.[33]

TABLE II
DSC Results of PCL and PCL/Clay Nanocomposites Before and After Foaming

Material	Before foaming		After foaming	
	T_c (°C)	χ_c (%)	T_c (°C)	χ_c (%)
PCL(SB)	20.5	43.9	28.8	37.0
PCL/Clay(SB)	30.6	49.7	34.3	42.7
PCL(ADC)	26.8	49.0	30.3	43.7
PCL/Clay(ADC)	26.1	49.0	28.0	41.0

polyacrylate/ZnO composites, where the addition of 14.3 wt % ZnO particles increased the degradation temperature of the polymer from 370 to 385°C. The degradation temperatures for the porous materials [Fig. 5(B)] appeared to present slightly lower values compared to the nonporous materials presumably because of the degradation of clay surfactants. However, similar to the nanocomposites before foaming, the addition of clay enhanced the degradation temperatures of the porous PCL from 355 to 396°C for porous PCL/Clay(SB) and from 380 to 387°C for porous PCL/Clay(ADC), confirming improvements in thermal properties with the incorporation of clay.

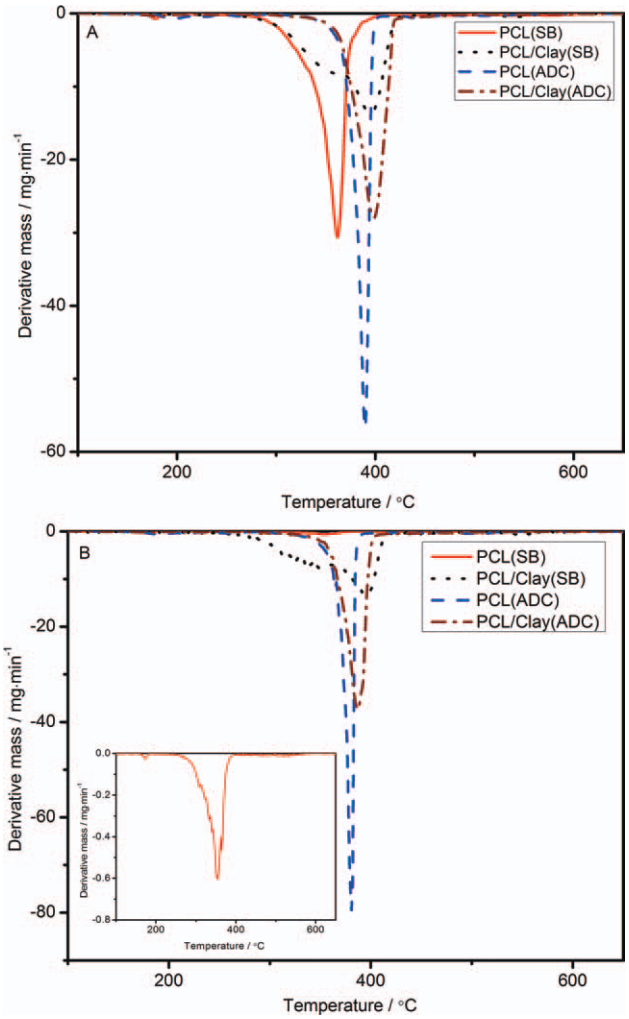

Figure 5 DTG curves of PCL and PCL/clay nanocomposites (A) before and (B) after foaming. [Color figure can be viewed in the online issue, which is available at wileyonlinelibrary.com.]

Mechanical properties

The compressive moduli and compressive stresses at 10% strain were determined via compressive testing performed on the foaming direction for porous PCL and PCL/clay nanocomposites, and the results are presented in Table III. The addition of clay exhibited a statistically significant increase in the modulus and stress of the porous polymer by 152 and 177% for ADC, which stems from the strong and stiff clay reinforcing filler, the strong interactions between the polymer and the clay and the reduced degree of crystallinity, porosity, and pore size. For SB as the blowing agent, the incorporation of clay increased the compressive stress of the porous PCL by 84% whilst maintaining a similar modulus. The effects of treated organoclays on the mechanical properties of porous PCL are further discussed by eliminating the effects of porosity (density) and plotting the relative modulus-relative density relationships for the porous nanocomposites. The blowing agent used also influenced the compressive properties: the modulus of the porous PCL diminished from 109.8 MPa for SB to 17.1 MPa for ADC due to different porosities and pore sizes formed.

To eliminate the effect of density, the specific compressive stress (the ratio of stress to density) and specific modulus (the ratio of modulus to density) were calculated, and the results are depicted in Figure 6. For ADC-treated organoclay, the specific modulus and specific compressive stress at 10% strain of the porous polymer were found to present statistically significant enhancements of 73 and 69% with the presence of clay. The addition of SB-treated clay presented an increase of 72% in the specific compressive strength. Thus, the improvements observed in the mechanical properties of porous PCL/clay nanocomposites are attributable to the good

TABLE III
Compressive Properties of Porous PCL and PCL/Clay Nanocomposites

Material	Compressive modulus (MPa)	Compressive stress at 10% strain (MPa)
PCL(SB) (P)	109.8 ± 31.8	4.3 ± 1.3
PCL/Clay(SB) (P)	92.0 ± 32.7	7.9 ± 4.4
PCL(ADC) (P)	17.1 ± 4.9	1.3 ± 0.4
PCL/Clay(ADC) (P)	43.1 ± 3.3	3.6 ± 0.1

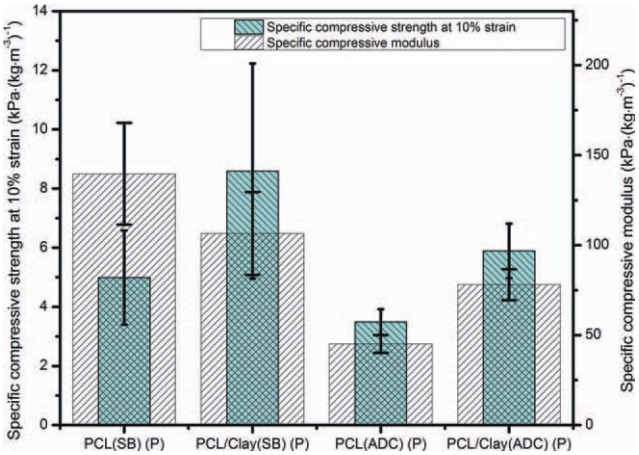

Figure 6 Specific compressive modulus and specific compressive stress at 10% strain of porous PCL and PCL/clay nanocomposites. [Color figure can be viewed in the online issue, which is available at wileyonlinelibrary.com.]

dispersion of the strong and stiff clay platelets inside the polymer matrix and the smaller pore size.

An enhancement in the compressive modulus of porous PCL/clay nanocomposites was previously reported by Liu et al.[12] who found that by premixing PCL with 5 wt % DK2 (3.5 wt % clay platelets)[40] followed by the addition of ADC the modulus of the porous PCL increased by $\sim$ 60%, while the specific compressive modulus presented an increase of close to 10%. At 5.8 wt % ADC-treated clay (i.e., 2.2 wt % clay platelets-calculated according to the equations presented in the Supporting Information section), we discovered that by pretreating the organoclay (C30B containing the same surfactant as that of DK2) with the blowing agent, the compressive modulus increased by 152%, while the specific compressive modulus was enhanced by 69%, compared to the pristine porous PCL(ADC). This showed that pretreating the clay with the blowing agent led to porous PCL/clay nanocomposites characterized by a higher degree of exfoliation and a greater decrement in pore size (46 vs. 43%),[12] which resulted in superior mechanical properties.

To examine the effect of foam and solid densities and the compressive modulus of the solid materials on the compressive modulus of porous materials, the relative moduli of the porous PCL/clay nanocomposites (compressive modulus for porous material or foam/compressive modulus for solid, E_f/E_s) were determined. A number of closed-cell models, based on eq. (2)[38] were tested.

$$\frac{E_f}{E_s} = C\left(\frac{\rho_f}{\rho_s}\right)^n \tag{2}$$

where E is the Young's modulus and ρ is the density, for which the subscripts s and f refer to the fully dense solid nanocomposite and porous or foam nanocomposite, respectively, C is a geometrical constant, and the exponent n is characteristic to the type of deformation that the struts encounter during compression, for example, bending, or axial stretching.[41]

The moduli for the solid nanocomposites were calculated according to the Mori–Tanaka model[42,43] and considering a compressive modulus for solid PCL of 324 MPa[44] and a modulus for clay platelets of 230 GPa.[45] The modulus for the solid polymer/clay nanocomposite with fully exfoliated clay platelets that occurred in PCL/Clay(SB) (P) was calculated to be 1360 MPa using the Mori–Tanaka model[42,43] (see the Supporting Information for details of the calculation). An aspect ratio of the reinforcing filler of 75, determined by measuring over 25 clay platelets in the TEM images and considering a 95% confidence interval, and an effective volume fraction of the reinforcing filler,[35] that is, the exfoliated clay platelets with a fraction of adsorbed polymer molecules behaving like the solid, of 0.06, were used for such calculation.

The modulus for the solid intercalated/exfoliated nanocomposite that occurred in PCL/Clay(ADC) (P) was determined by considering that the nanomaterial included two different nanocomposite systems, that is, intercalated and exfoliated. The intercalated nanosystem was assumed to occur in 25% of the polymer matrix with the exfoliated one distributing in the rest of the matrix, on the basis that the ratio of the number of intercalated platelets to the total number of clay platelets in the nanocomposite was 0.4 and that two platelets made up one intercalated tactoid. The modulus of the solid exfoliated nanocomposite was calculated, according to the Mori–Tanaka model[42,43] with the application of the effective volume fraction, to be 878 MPa. The modulus of the solid intercalated nanocomposite was determined, using the Mori–Tanaka model[42,43] and considering the intercalated clay tactoid as the reinforcing filler, as 444 MPa. Using the rule of mixtures, the modulus of the solid intercalated/exfoliated nanocomposite was determined as 769 MPa. Details of these calculations are available in the Supporting Information.

By inserting the values of relative density and solid moduli calculated above into eq. (2), where C and n differ with various models for closed cells,[46–51] it was found that the Mills–Zhu model,[47] described by eq. (3), gives the best predictions for the experimental data and was therefore presented in Figure 7. Other models tested[46–51] gave unreasonable predictions of the experimental data. The Mills–Zhu model was developed based on Clutton and Rice's data[52] for LDPE and only underestimated the experimental data by 16% for PCL/Clay(SB) (P) and by 43% for PCL/Clay(ADC) (P).

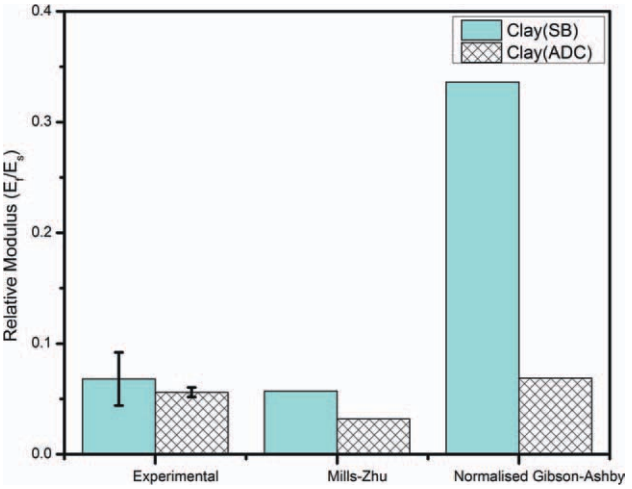

Figure 7 Theoretical and experimental data of relative Young's modulus versus relative density for porous PCL/clay nanocomposites. [Color figure can be viewed in the online issue, which is available at wileyonlinelibrary.com.]

$$\frac{E_f}{E_s} = 0.0807\left(\frac{\rho_f}{\rho_s}\right)^{1.155} \quad (3)$$

The predicted results from the normalized Gibson–Ashby model[37,38,53] described by eq. (4) and used to depict the relative density-relative modulus relationship in low-density polymer/clay nanocomposite foams were also presented in Figure 7.

$$\frac{E_f}{E_s} = C_1\phi_s^2\left(\frac{\rho_f}{\rho_s}\right)^2 + C_2(1-\phi_s)\frac{\rho_f}{\rho_s} \quad (4)$$

where C_1 and C_2 are geometrical constants and ϕ_s is the volume fraction of the solid contained in the foam.

For the normalized Gibson–Ashby model,[37,38,53] the volume fraction of the solid contained in the foam was estimated from the foam and solid densities for each porous material (Table I).[54] This model presented different variations for the treated clays, highly overestimating the experimental datum for PCL/Clay(SB) (P) while only overestimating the experimental modulus of PCL/Clay(ADC) (P) by 22%. These variations are due to the fact that in porous solids with a porosity lower than 70%,[38] the solid is located both in the edges and in the faces of cells and not mostly in the cell edges as it is expected for low-density foams, with a porosity higher than 95%.[55] As a result, porosity along with cell structure constitutes a key factor in governing the relative density-relative modulus relationships for foams.[37,38]

Overall, the reasonably good agreement between the experimental data and the theoretical values predicted using the Mills–Zhu model[47] suggests that this model can be used to design the mechanical properties of the porous nanocomposites.

CONCLUSION

Highly exfoliated porous PCL/clay nanocomposites were prepared using a novel method by inserting the blowing agent into the galleries of an organoclay before nanocomposite formation to render the blowing agent dual roles in the foaming process, that is, formation of bubbles and facilitation of clay exfoliation. SB and ADC were used as the blowing agents, and their entrance into clay galleries was confirmed by FTIR. The insertion of the blowing agent into clay galleries before foaming improved the exfoliation degree of clay in PCL substantially, as characterized using XRD and TEM, resulting in fully exfoliated PCL/Clay(SB) and highly dispersed PCL/Clay (ADC) porous solids. The addition of clay controlled the nucleation and cell growth, decreasing the pore size by 39–46% and leading to the occurrence of more uniform cell structures.

Thermal analysis results showed that for SB the crystallinity of the porous PCL increased from 37 to 42.7% due to the nucleating effect of the exfoliated clay platelets, while the degradation temperature increased by 41°C. Although very small amounts of clay platelets were used, that is, 2.2 and 2.9 wt %; the compressive modulus and stress at 10% strain of the porous polymer were found to increase by up to 152 and 177%, respectively. Eliminating the effect of the density, the specific compressive modulus remained up to 73% higher than that of the porous PCL, while the specific compressive stress at 10% strain improved by up to 69%. The relative density-relative modulus relationship was found to be best described by the Mills–Zhu model for closed-cell structures. These biocompatible porous solids are expected to find applications in biodegradable packaging and carriers of drugs, chemicals, and medical and diagnostic devices.

Ms. Judith Greaney is thanked for the participation in sample preparation and compression tests and Mr. Peter O'Reilly is thanked for help with setting up the compression tests.

References

1. Federle, T. W.; Barlaz, M. A.; Pettigrew, C. A.; Kerr, K. M.; Kemper, J. J.; Nuck, B. A.; Schechtman, L. A. Biomacromolecules 2002, 3, 813.
2. Queiruga, D.; Walther, G.; González-Benito, J.; Spengler, T. Waste Manage 2008, 28, 181.
3. Wei, M.; Shuai, X.; Tonelli, A. E. Biomacromolecules 2003, 4, 783.
4. Sangwan, P.; Way, C.; Wu, D.-Y. Macromol Biosci 2009, 9, 677.

5. Barsema, J. N.; Bostoen, C. L.; Jansen, R. H. S.; Mulder, M. H. V.; Nauta, W. J.; Steeman, P. A. M.; Wessling, M. Macromolecules 2003, 36, 6817.
6. Mori, T.; Hayashi, H.; Okamoto, M.; Yamasaki, S.; Hayami, H. Compos A 2009, 40, 1708.
7. Nam, P. H.; Maiti, P.; Okamoto, M.; Kotaka, T.; Nakayama, T.; Takada, M.; Ohshima, M.; Usuki, A.; Hasegawa, N.; Okamoto, H. Polym Eng Sci 2002, 42, 1907.
8. Arora, K. A.; Lesser, A. J.; McCarthy, T. J. Macromolecules 1998, 31, 4614.
9. Diaz, C. A.; Matuana, L. M. J Vinyl Addit Technol 2009, 15, 211.
10. Zhang, Q.; Xanthos, M.; Dey, S. K. J Cell Plast 2001, 37, 284.
11. DiMaio, E.; Mensitieri, G.; Iannace, S.; Nicolais, L.; Li, W.; Flumerfelt, R. W. Polym Eng Sci 2005, 45, 432.
12. Liu, H.; Han, C.; Dong, L. J Appl Polym Sci 2010, 115, 3120.
13. Lee, S. T.; Kareko, L.; Jun, J. J Cell Plast 2008, 44, 293.
14. Quinn, S. Plast Addit Compound 2001, 3, 16.
15. Sims, G. L. A.; Sirithongtaworn, W. Cell Polym 1997, 16, 271.
16. Sims, G. L. A.; O'Connor, C. In Blowing Agent Systems: Formulations and Processing; Limited, R. T., Ed.; Smithers Rapra Publishing: Shawbury, Shrewsbury, UK, 1998; p1.
17. Mangiacapra, P.; Raimondo, M.; Tammaro, L.; Vittoria, V.; Malinconico, M.; Laurienzo, P. Biomacromolecules 2007, 8, 773.
18. Ludueña, L. N.; Alvarez, V. A.; Vazquez, A. Mater Sci Eng A 2007, 460–461, 121.
19. Pavlidou, S.; Papaspyrides, C. D. Prog Polym Sci 2008, 33, 1119.
20. Chen, B.; Evans, J. R. G. Macromolecules 2006, 39, 747.
21. Ozkoc, G.; Kemaloglu, S.; Quaedflieg, M. Polym Compos 2010, 31, 674.
22. Chen, B.; Evans, J. R. G.; Greenwell, H. C.; Boulet, P.; Coveney, P. V.; Bowden, A. A.; Whiting, A. Chem Soc Rev 2008, 37, 568.
23. Marrazzo, C.; Di Maio, E.; Iannace, S. J Cell Plast 2007, 43, 123.
24. Ding, M.; Li, J.; Fu, X.; Zhou, J.; Tan, H.; Gu, Q.; Fu, Q. Biomacromolecules 2009, 10, 2857.
25. Robledo-Ortiz, J. R.; Zepeda, C.; Gomez, C.; Rodrigue, D.; González-Núñez, R. Polym Test 2008, 27, 730.
26. De Kesel, C.; Lefèvre, C.; Nagy, J. B.; David, C. Polymer 1999, 40, 1969.
27. Kuila, B. K.; Nandi, A. K. Macromolecules 2004, 37, 8577.
28. Singhal, R.; Datta, M. Polym Compos 2009, 30, 887.
29. Chen, G. M.; Liu, S. H.; Chen, S. J.; Qi, Z. N. Macromol Chem Phys 2001, 202, 1189.
30. Socrates, G. Infrared and Raman Characteristic Group Frequencies: Tables and Charts; Wiley: Chichester, 2001.
31. Dodds, W. S.; Stutzman, L. F.; Sollami, B. J. Ind Eng Chem Chem Eng Data 1956,92.
32. Lee, L. J.; Zeng, C.; Cao, X.; Han, X.; Shen, J.; Xu, G. Compos Sci Technol 2005, 65, 2344.
33. Baker, S. C.; Rohman, G.; Southgate, J.; Cameron, N. R. Biomaterials 2009, 30, 1321.
34. Lu, C.; Mai, Y.-W. Phys Rev Lett 2005, 95, 088303.
35. Chen, B.; Evans, J. R. G. Macromolecules 2006, 39, 1790.
36. Kawasumi, M.; Hasegawa, N.; Kato, M.; Usuki, A.; Okada, A. Macromolecules 1997, 30, 6333.
37. Mills, N. J. Polymer Foams Handbook—Engineering and Biomechanics Applications and Design Guide; Elsevier: Oxford, 2007.
38. Gibson, L. J.; Ashby, M. F. Cellular Solids: Structure and Properties; Cambridge University Press: Cambridge, 1997.
39. Liufu, S.-C.; Xiao, H.-N.; Li, Y.-P. Polym Degrad Stab 2005, 87, 103.
40. Feyz, E.; Jahani, Y.; Esfandeh, M. Macromol Symp 2011, 298, 130.
41. Jain, A.; Rogojevic, S.; Gill, W. N.; Plawsky, J. L.; Matthew, I.; Tomozawa, M.; Simonyi, E. J Appl Phys 2001, 90, 5832.
42. Mori, T.; Tanaka, K. Acta Metall 1973, 21, 571.
43. Tandon, G. P.; Weng, G. J. Polym Compos 1984, 5, 327.
44. Chen, B. PhD Thesis, University of London, 2005.
45. Chen, B.; Evans, J. R. G. Scripta Mater 2006, 54, 1581.
46. Andrews, E.; Sanders, W.; Gibson, L. J. Mater Sci Eng A 1999, 270, 113.
47. Mills, N. J.; Zhu, H. X. J Mech Phys Solids 1999, 47, 669.
48. Renz, R.; Ehrenstein, G. W. Cell Polym 1982, 1, 5.
49. Simone, A. E.; Gibson, L. J. Acta Mater 1998, 46, 2139.
50. Weaire, D.; Phelan, R. J Phys-Condens Mater 1996, 8, 9519.
51. Roberts, A. P.; Garboczi, E. J. Acta Mater 2001, 49, 189.
52. Clutton, E. Q.; Rice, G. N. Cell Polym 1992, 11, 429.
53. Istrate, O. M.; Chen, B. Soft Matter 2011, 7, 1840.
54. Ruike, M.; Kasu, T.; Setoyama, N.; Suzuki, T.; Kaneko, K. J Phys Chem 1994, 98, 9594.
55. Gibson, L. J.; Ashby, M. F. Proc R Soc London Ser A 1982, 382, 43.